Heterocycles

International Edition: DOI: 10.1002/anie.202000556
German Edition: DOI: 10.1002/ange.202000556

BN-Embedded Polycyclic Aromatic Hydrocarbon Oligomers: Synthesis, Aromaticity, and Reactivity

*Yijing Chen, Weinan Chen, Yanjun Qiao, Xuefeng Lu, and Gang Zhou**

Abstract: *BN-embedded oligomers with different pairs of BN units were synthesized by electrophilic borylation. Up to four pairs of BN units were incorporated in the large polycyclic aromatic hydrocarbons (PAHs). Their geometric, photophysical, electrochemical, and Lewis acidic properties were investigated by X-ray crystallography, optical spectroscopy, and cyclic voltammetry. The B–N bonds show delocalized double-bond characteristics and the conjugation can be extended through the trans-orientated aromatic azaborine units. Calculations reveal the relatively lower aromaticity for the inner azaborine rings in the BN-embedded PAH oligomers. The frontier orbitals of the longer oligomers are delocalized over the inner aromatic rings. Consequently, the inner moieties of the BN-embedded PAH oligomers are more active than the outer parts. This is confirmed by a simple oxidation reaction, which has significant effects on the aromaticity and the intramolecular charge-transfer interactions.*

Introduction

Polycyclic aromatic hydrocarbons (PAHs) have attracted tremendous interest because of their extensive applications in optoelectronic devices, such as light-emitting diodes (LEDs),[1] field-effect transistors (FETs),[2] and organic photovoltaics (OPVs).[3] The development of heteroatom-substituted PAHs has been a hot topic in the past decade since they are useful and indispensable elements to acquire novel materials with unique properties and tailored functions.[4] Among a variety of possible dopants, boron and nitrogen have received particular attention owing to their distinct electronic and optical characteristics.[5] One popular strategy for doping both boron and nitrogen into PAHs is substituting one or more C=C units by B–N units, which can be considered as zwitterionic double bonds in the neutral state.[6] The replacement of a C=C bond by an isosteric and isoelectronic B–N bond not only expands the structural diversity of organic conjugated materials but also enriches the fundamental understanding of the aromaticity.[7] Moreover, some BN-embedded PAHs exhibit distinct electronic and optical properties, making them promising candidates for various optoelectronic applications.[8] The azaborine chemistry has been well-established by several groups[9] In general, most nucleophilic borylation requires a strong base, such as butyllithium.[10] However, the basic character of organolithium reagents may cause undesired side reactions, limiting the range of structural modifications. Moreover, the limited solubility of intermediate aryllithium in organic solvents makes it more difficult to access PAHs with multiple BN units.

Conjugated oligomers, which possess distinct electronic properties and facilitate the understanding of the fundamental structure–property relationship, are particularly desired for both chemistry and material scientists.[11] However, little research has focused on the conjugated oligomers with multiple BN units, which is probably due to the lack of a suitable method.[12] Although significant progress has been achieved in azaborine chemistry, extending the BN-doped heteroaromatics to much larger π-conjugated systems and the construction of BN-embedded PAH oligomers still remain challenging.

Herein, we report a strategy to construct BN-embedded PAH oligomers BN1–BN4 (Figure 1) by electrophilic borylation approach, which avoids the use of organolithium intermediates. Therefore, large polycyclic aromatic hydrocarbons with multiple pairs of BN units can be facilely realized. The embedded BN units are in *trans*-orientation in these PAH oligomers. Benzene and thiophene rings are fused on the 1,2-azaborine rings. Their geometric, photophysical, electrochemical, and Lewis acidic properties have been systematically investigated by X-ray crystallography, optical

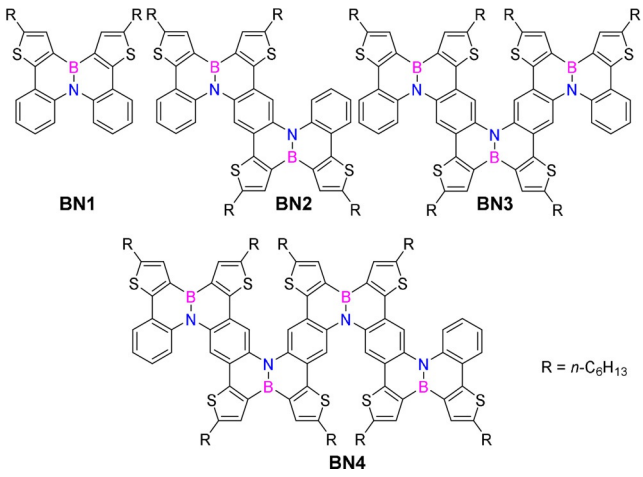

Figure 1. Chemical structures of BN-embedded PAH oligomers BN1–BN4.

[*] Dr. Y. Chen, W. Chen, Prof. Dr. G. Zhou
Lab of Advanced Materials, State Key Laboratory of Molecular Engineering of Polymers, Fudan University
Shanghai 200438 (P. R. China)
E-mail: zhougang@fudan.edu.cn
Dr. Y. Qiao, Prof. Dr. X. Lu
Department of Materials Science, Fudan University
Shanghai 200438 (P. R. China)
Supporting information and the ORCID identification number(s) for the author(s) of this article can be found under: https://doi.org/10.1002/anie.202000556.

spectroscopy, and cyclic voltammetry measurements. Theoretical calculations were also performed to gain further insight into the aromaticity properties and molecular orbitals of the BN-embedded PAH oligomers. It is found that the B–N bonds show delocalized double-bond characteristics, but weaker than C=C bonds. Moreover, the molecular orbitals tend to delocalize on the conjugated skeletons through C=C bonds instead of azaborine rings. Consequently, the inner moieties of the BN-embedded PAH oligomers are more active than the two terminal parts. This assumption was further confirmed by a simple oxidation reaction and the product was verified by single crystal X-ray analysis. Interestingly, unlike the BN-embedded oligomers, remarkable intramolecular charge transfer (ICT)[13] interactions can be found in the oxidized products.

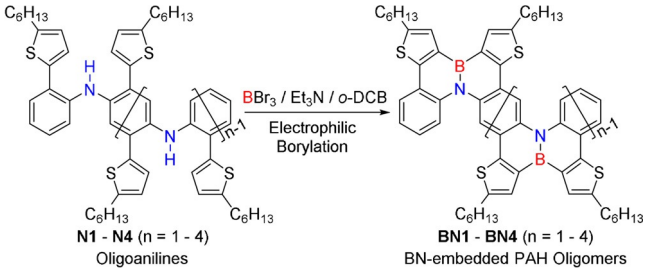

Scheme 1. Borylation of oligoanilines into BN-embedded PAH oligomers.

Results and Discussion

Synthesis and Structure Characterization

The synthetic approach to BN-embedded PAHs BN1–BN4 involved a construction of oligoaniline precursors N1–N4 and ended by an electrophilic borylation[14] in the presence of boron bromide and triethylamine (Scheme 1). To prepare the oligomeric precursors, palladium-catalyzed Buchwald[15] and Suzuki[16] coupling reactions are alternately conducted to construct the oligoaniline backbones. As shown in Scheme 2, the synthesis of precursors N1 and N2 both started from 2-bromoaniline (**1**), which was directly converted to bis(2-bromophenyl)amine (**2**) and 2,5-dibromo-*N*,*N*′-bis(2-bromophenyl)benzene-1,4-diamine (**3**), respectively, via Buchwald coupling reaction. Then precursors N1 and N2 were produced by Suzuki coupling of **2** or **3** and 2-(5-hexylthienyl)-4,4,5,5-tetramethyl-1,3,2-dioxaborolane. For precursors N3 and N4, to avoid the side reactions and simplify the synthesis, partial pendant hexylthienyl groups were incorporated initially. As shown in Scheme 2, the synthetic route for precursors N3 and N4 both began with 2,5-bis(5-hexylthienyl)-1,4-phenylenediamine (**4**), which was prepared according to a previous report.[17] After two asymmetric Buchwald coupling with 2-(2-bromophenyl)-5-hexylthiophene and 2,5-dibromo-*N*-(2-(5-hexylthienyl)phenyl)-4-iodoaniline, the corresponding trimer backbone (**6**) was provided and further converted into precursor N3 by attaching two pendant hexylthienyl groups. Similarly, the skeleton of the tetramer **7** was afforded by a symmetric Buchwald coupling reaction of compound **4** and

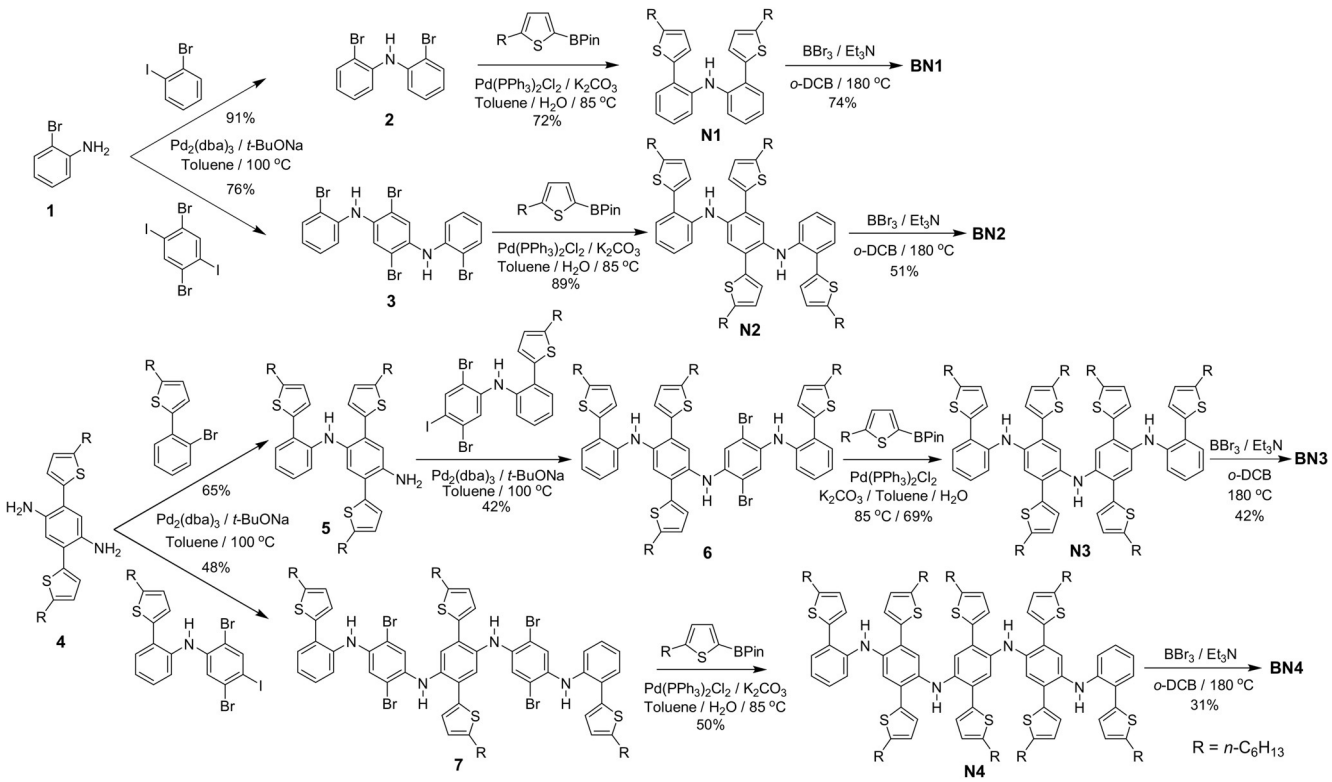

Scheme 2. Synthetic routes for BN-embedded PAH oligomers BN1–BN4.

2.2 equiv of 2,5-dibromo-*N*-(2-(5-hexylthienyl)phenyl)-4-iodoaniline. Then, the pendant hexylthienyl groups were attached on the backbone of the tetramer via Suzuki coupling reaction. Finally, the oligoaniline precursors N1–N4 were converted into PAH oligomers BN1–BN4 by refluxing with boron bromide and triethylamine in *o*-dichlorobenzene. The yield of the oligomers decreased from 74% to 31% with the increasing number of BN pairs obviously due to the enhanced borylation sites. The target compounds were characterized by ^{1}H NMR, ^{13}C NMR, and HRMS spectroscopy, and were found to be consistent with the proposed structures. Furthermore, MALDI-TOF mass spectra (Figure 2) exhibited single intense signals corresponding to the calculated masses of the BN-embedded PAH oligomers.

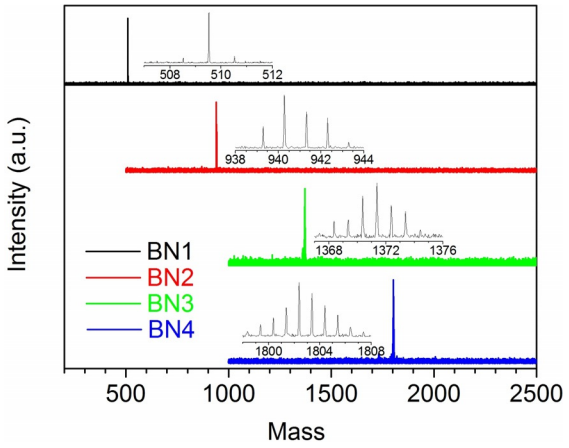

Figure 2. MALDI-TOF mass spectra with expanded views of the molecular-ion regions of BN-embedded PAH oligomers BN1–BN4.

To verify the successful doping of BN units into the PAHs and investigate the molecular structural features, single-crystal X-ray diffraction analysis was performed for BN1 and BN2. The single crystal of BN1 was obtained as white lamellar crystal by diffusion of hexane into its chloroform solution and slow evaporation at room temperature. Single-crystal X-ray analysis (Figure 3; Supporting Information, Table S1) demonstrates that the molecules of BN1 are aligned in a triclinic unit cell. The length of the B–N bond is 1.4555(18) Å (Figure 3b), which is shorter than the value for a B–N single bond (1.58 Å),[18] but longer than a localized B=N double bond (1.40 Å).[19] These data indicate the presence of the delocalized BN double bond character and the effective conjugation extension through the BN bond. On the other hand, the bond length of the adjacent N1–C1, N1–C17, B1–C8, and B1–C24 is 1.4271(16), 1.4285(17) 1.530(2), and 1.5306(19) Å, respectively, suggesting the characteristics of single bonds. While C1–C6 (1.4172(19) Å), C7–C8 (1.3786-(18) Å), C17–C22 (1.4148(18) Å), and C23–C24 (1.3801-(18) Å) bonds in the azaborine rings all exhibit as delocalized double bonds, which indicates the aromaticity of the two azaborine rings and is further supported by nucleus-independent chemical shift (NICS) calculations.[20] Moreover, as shown in Figure 3c, the two azaborine rings in BN1 are

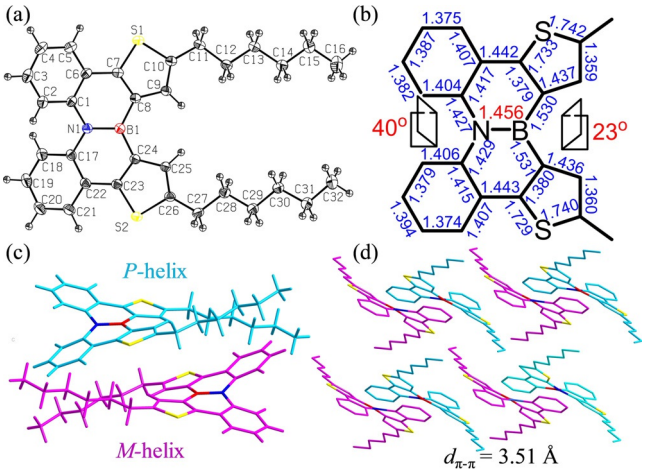

Figure 3. a) ORTEP drawing of BN1 with ellipsoids set at 50% probability. b) Selected bond lengths for BN1. c) *P*- and *M*-helical structures of BN1. d) Crystal packing of BN1 (Hydrogen atoms are omitted for clarity).[30]

slightly twisted due to the steric repulsion between the hydrogen atoms at the *ortho* positions of the heteroatoms. The dihedral angle between the two thiophene rings fused on the azaborine units is measured to be 23°. While the dihedral angle between the two benzene rings is 40°. It is interesting to note that two different conformations can be found in the same crystal. Each space unit contains a couple of *P*- and *M*-helical structures with BN dipole moments opposite to each other (Figure 3c). Furthermore, the molecules are arranged in an offset head-to-tail stacking array along the *c* axis (Figure 3d). The π–π distance between *P*-helix and *M*-helix is around 3.51 Å, which agrees with the fact that BN1 possesses an extended π-conjugated backbone through the two azaborine rings.

Unfortunately, the single crystal of BN2 was not successfully obtained probably owing to the interruption of the packing structures by the four hexyl chains. To provide further insight into the chemical structures of the BN-embedded oligomers, the hexyl substituents in BN2 were shortened to methyl groups and analogue Me-BN2 was synthesized similarly (Supporting Information, Scheme S2). A single crystal suitable for X-ray crystallography was grown by slow evaporation of acetone into the solution of Me-BN2 in carbon disulfide. As shown in Figure 4b, the bond lengths of the two B–N bonds were 1.447(3) and 1.454(3) Å, displaying as delocalized double bonds, similar to that in BN1. Moreover, the bond lengths of C10–C11 (1.436(3) Å) and C33–C34 (1.434(3) Å) in the outer azaborine rings are slightly shorter than those of C4–C5 (1.443(3) Å) and C23–C25 (1.442(3) Å) in the inner azaborine rings, indicating the different charge delocalization effects and aromaticity between the outer and inner azaborine rings. Furthermore, Me-BN2 has four cove regions. Two types of distortions can be found due to the different steric hindrances of hydrogen atoms on the benzene and thiophene rings. The dihedral angle between the benzene rings fused on the azaborine units are 33° and 36°, respectively, while the dihedral angles between the two thiophene rings are 8° and 17°, respectively (Figure 4b). Additionally, *P*-

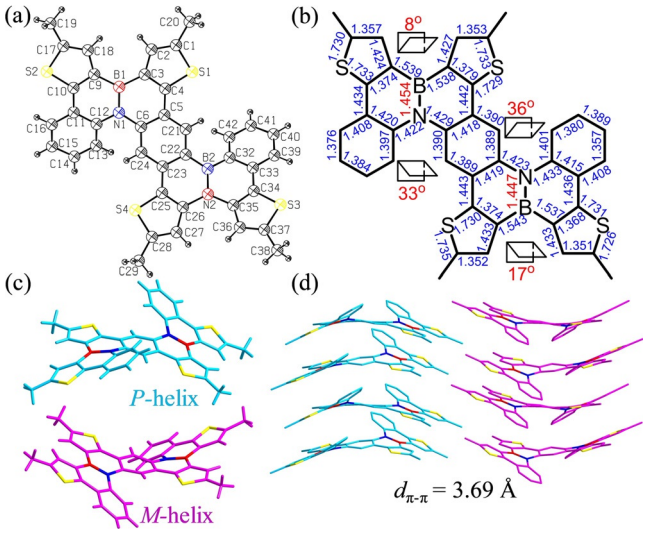

Figure 4. a) ORTEP drawing of Me-BN2 with ellipsoids set at 50% probability. b) Selected bond lengths for Me-BN2. c) *P*- and *M*-helical structures of Me-BN2. d) Crystal packing of Me-BN2 (Hydrogen atoms are omitted for clarity).[30]

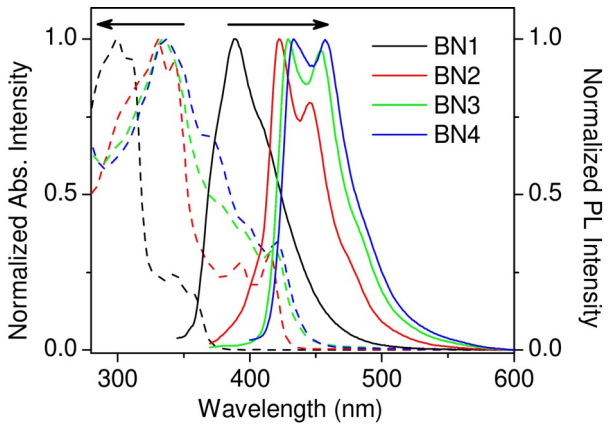

Figure 5. UV/Vis absorption (-----) and PL spectra (——) of the BN-embedded PAH oligomers BN1–BN4 in THF solutions (10^{-6} M).

and *M*-helical structures (Figure 4c) can be also found in the single crystal of Me-BN2. Unlike BN1, the *P*- and *M*-helical structures in Me-BN2 form separated arrays. The π–π distances in the two arrays are both 3.69 Å (Figure 4d), which is slightly higher than that in BN1 and owing to the more twisted structures of Me-BN2.

Photophysical Properties

The photophysical properties of BN-embedded PAH oligomers BN1–BN4 in THF solutions (ca. 10^{-6} M) were investigated by UV/Vis absorption and photoluminescence (PL) spectroscopy (Figure 5 and Table 1). All the PAHs exhibit two distinct absorption bands. The intense absorption band in the high energy region typically originates from the $S_0 \rightarrow S_2$ transition and the rather weak shoulder in low energy region can be assigned to the $S_0 \rightarrow S_1$ transition. As shown in Figure 5, the maximum absorption wavelength of BN1 locates at 357 nm. Upon increasing the number of the BN units, the absorption maximum gradually shifts to 415, 419, and 420 nm for BN2, BN3, and BN4, respectively. The bathochromic shift among the PAH oligomers stepwise reduced from 58 to 4 nm and further to 1 nm. This is obviously due to the extension of the effective conjugation length, which is a well-known behavior in conjugated oligomers.[21] Moreover, with the increasing oligomer length, the absorption shoulder in low energy region gradually increases. Originally, the $S_0 \rightarrow S_1$ transition is symmetry forbidden. However, upon extending the PAH framework, the molecular symmetry is reduced, thus increasing the oscillator strength of the $S_0 \rightarrow S_1$ transition.[22] Under the same conditions, the corresponding PL spectra of BN1–BN4 are peaked at 388, 422, 429, and 433 nm with a vibronic shoulder around 411, 445, 454, and 457 nm, respectively, which can be assigned to the 0-0 and 0-1 singlet transitions and indicates that the effective conjugation length is not saturated in the BN-embedded PAH tetramer. With the number of BN units increasing, the intensity of the shoulder peak increases stepwise, which suggests that the 0-1 singlet transition is activated in a longer conjugation system due to the enhanced electron transition rate. Moreover, the bathochromic shifts in the PL spectra among the PAH oligomers are 34, 7, and 4 nm, respectively, which are different from those in corresponding absorption spectra. This suggests that the backbone geometry changes significantly between the ground state and the vibronically relaxed excited state.

It is well known that the presence of arylamine donors and arylborane acceptors result in remarkable charge transfer (CT) characteristics. To further investigate the CT interactions in the BN-embedded PAHs, the solvatochromic effects on the absorption and PL features were investigated (Supporting Information, Figures S1 and S2). The four PAHs exhibit relatively weak solvatochromism (λ_{max} shift < 13 nm

Table 1: Photophysical Data of BN-embedded PAHs BN1–BN4.

Comp.	λ_{abs} [nm][a]	ε [10^4 M^{-1} cm^{-1}]	λ_{abs} [nm][b]	λ_{PL} [nm][a]	λ_{PL} [nm][b]	Stokes shift [cm^{-1}]	E_g [eV][c]	E_{onset} [V]	E_{HOMO} [eV][d]	E_{LUMO} [eV][e]
BN1	357	0.8	366	388	421	689	3.22	0.58	−5.38	−2.16
BN2	415	1.3	420	422	468	400	2.81	0.48	−5.28	−2.47
BN3	419	3.0	425	429	496	556	2.71	0.44	−5.24	−2.53
BN4	420	4.4	427	433	504	715	2.66	0.42	−5.22	−2.56

[a] Absorption (λ_{abs}) and PL (λ_{PL}) maxima were measured in THF solutions (10^{-6} M). [b] Absorption (λ_{abs}) and PL (λ_{PL}) maxima were measured on quartz substrates. [c] E_g is optical band gap. [d] Calculated from the onset of the first oxidation potential. $E_{HOMO} = -(E_{onset} + 4.80)$ eV. [e] $E_{LUMO} = E_g + E_{HOMO}$.

when solvents ranging from hexane to DMF). This indicates that the CT interactions in the BN-embedded PAH oligomers are rather poor, which may be a result of the delocalized BN double-bond characteristics of the oligomers.

In contrast to the absorption spectra in THF solutions, the films of BN1–BN4 display maximum absorption wavelengths at 366, 420, 425, and 427 nm, respectively (Supporting Information, Figure S3a). A bathochromic shift of 9, 5, 6, and 7 nm can be observed in comparison to those in THF solutions, which is attributed to the π–π stacking interactions among the PAH molecules in solid states. Under the same conditions, the PL maxima of BN1–BN4 locates at 421, 468, 496, and 504 nm, respectively (Supporting Information, Figure S3b). A distinct bathochromic shift of 33, 46, 67, and 71 nm can be observed in comparison to those in THF solutions, which are much larger than those in corresponding absorption spectra and probably owing to the formation of excimers upon excitation.

Coordination with Fluoride Ions

It is well known that three-coordinate boron contains an empty orbital, which can be occupied by a Lewis base.[23] To study their Lewis acidic properties, the BN-embedded PAH oligomers were titrated with fluoride ions by monitoring their absorption and PL spectra. Upon addition of tetra-*n*-butylammonium fluoride (TBAF) to the solutions of the BN oligomers in THF (ca. 10^{-6} M), distinct bathochromic shifts can be observed for both absorption and PL maxima of the BN oligomers. As shown in the Supporting Information, Figure S4, the maximum absorption wavelengths of BN1–BN4 shift from 357, 415, 419, and 420 nm to 385, 435, 461, and 480 nm, respectively, after adding excess fluoride ions. Similarly, stepwise addition of TBAF to the oligomer solutions bathochromically shift their PL maxima from 388, 422, 429, and 433 nm to 438, 490, 510, and 530 nm by 50, 68, 81, and 97 nm, respectively (Supporting Information, Figure S5). All the absorption and PL changes indicate the appearance of the F-BN complexes and originate from the occupation of the empty orbitals of the boron atoms by fluoride ions. It should be noted that the bathochromic shifts for the longer oligomers are more remarkable than the shorter ones probably owing to the more coordination sites in the longer oligomers. Therefore, more significant fluorescence changes can be found for longer oligomers by the naked eye upon addition of TBAF. As shown in Figure 6, no obvious color change can be observed for BN1, while the fluorescence of the BN2, BN3, and BN4 change from blue to bluish green, green, and pale yellow. Moreover, the emission colors of all oligomers can be recovered to their original states after adding one drop of water owing to the decomposition of the fluoride-coordinated boron anions.

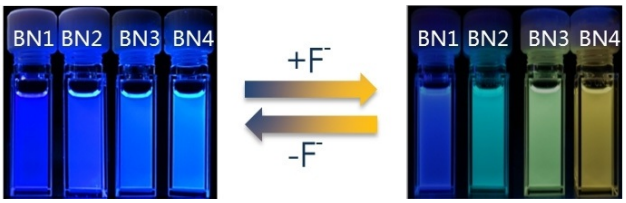

Figure 6. Emission images of the BN-embedded PAH oligomers in THF solutions upon addition of Bu_4NF.

To gain insight into the electrochemical behaviors of the BN-embedded PAH oligomers BN1–BN4 and their fluoride-coordinated complexes, cyclic voltammetry (CV) measurements were conducted in anhydrous DCM. As depicted in Table 1 and the Supporting Information, Figure S6, all the oligomers exhibit irreversible oxidation processes, and the oxidation onsets locate at 0.58, 0.48, 0.44, and 0.42 V (vs. Fc^+/Fc) for BN1, BN2, BN3, and BN4, respectively. Correspondingly, the highest occupied molecular orbital (HOMO)[24] energy level gradually lifts up from −5.38 eV for BN1 to −5.22 eV for BN4 as the number of BN units increases. While the LUMOs of the oligomers are −2.16, −2.47, −2.53 and −2.56 eV, respectively. Consequently, with the π-conjugation extension in the BN-embedded oligomers, the HOMO levels gradually increase while the LUMO level dramatically decreases, resulting in stepwise reduced band gap. This suggests the conjugation extension through the azaborine rings and the charge delocalization in the BN-embedded PAH oligomers. When the boron in the azaborine is coordinated by fluoride ion, the onsets of the first oxidation potentials of BN1–BN4 locate at −0.06, −0.13, −0.32, and −0.37 V (Supporting Information, Figure S7). A significant negative shift can be found for all the oligomers, which is attributed to the anionic four-coordinate boronate converted from an electron acceptor into a strong electron donor. Moreover, a more significant shift of the first oxidation potential can be observed for the longer oligomers. This originates from the more coordination sites in the longer oligomers, resulting in more negative charge after coordinating fluoride ions.

Theoretical Approaches

To further understand the aromaticity of the BN-embedded PAH oligomers, NICS calculations were carried out. As shown in Figure 7, the two azaborine rings in BN1 show a NICS(1)[25] value of −4.1 ppm, which is higher than that for the reported BN-fused dibenzo[*g,p*]chrysene (−2.9 ppm).[7a] These results suggested that the incorporation of thiophene ring instead of benzene ring has indeed successfully improved the aromaticity of the azaborine ring. Most interestingly, with the extension of the oligomer length, the NICS(1) values of the azaborine rings exhibit two different sets of values in each oligomer. The NICS(1) values of the two terminal azaborine rings are ranged between −4.0–−4.2 ppm, while −3.5–−3.7 ppm for the other inner azaborine rings embedded in the molecules. This indicates that the aromaticity of the terminal azaborine rings are higher than the other inner rings. One plausible explanation is that the benzene ring neighboring the terminal azaborine unit is much easier to resonate as compared with the one fixed between two inner azaborine rings. Consequently, the double bonds between the terminal azaborine unit and the neighboring benzene ring may have larger bond resonance energy than the corresponding one in the inner azaborine rings, which thus contributes to the higher

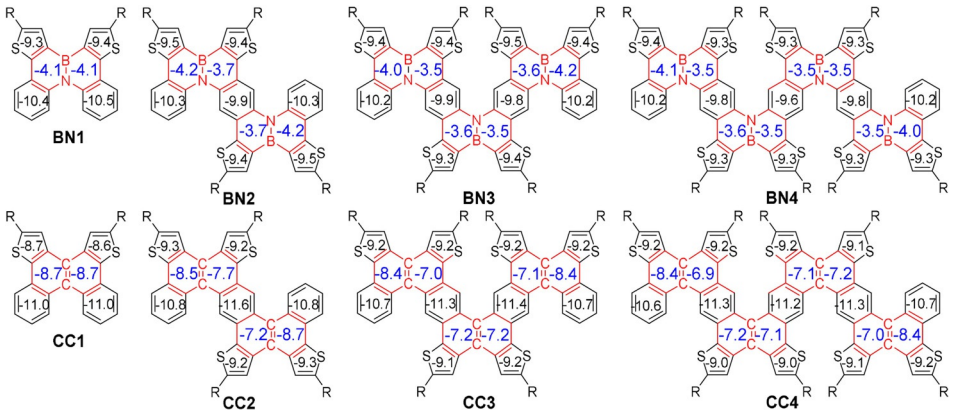

Figure 7. Calculated NICS(1) values [ppm] of BN-embedded PAH oligomers BN1–BN4 and corresponding isoelectronic carbon analogues CC1–CC4.

aromaticity for the two terminal azaborine rings in comparison to the other inner rings.[26] Although the aromaticity of the azaborine rings in these BN-embedded PAHs are relatively lower than the corresponding aromatic rings in the related isoelectronic carbon analogs (Figure 7), on the other hand, only negligible changes can be observed for the NICS(1) values of the benzene and thiophene rings neighboring to the azaborine ring as compared with those for the C=C analogues, suggesting that the borylation has little influence on the aromaticity of the surrounded aromatic rings.

Density functional theory (DFT) calculations[27] were also performed at the B3LYP/6-31G(d) level to learn the electronic properties of the BN-embedded PAH oligomers. As shown in Figure 8, the LUMO of BN1 delocalizes over the whole aromatic skeleton, while the HOMO has no weight at the boron atom. Unlike previously reported heteroatom-substituted PAHs containing separated boron and nitrogen where the charge can facilely transfer from the nitrogen center to the boron center,[28] only slight charge separation can be found in BN1, which results in the weak charge transfer interactions in azaborine containing compounds.[29] Similarly, with the BN-conjugation extension, oligomers BN2, BN3, and BN4 demonstrate delocalized HOMOs but without any distribution on the boron atoms. Moreover, both HOMOs and LUMOs of oligomers BN2, BN3, and BN4 are partially delocalized over the inner aromatic rings with ignorable weights on the two terminal sides. These results suggest that the inner aromatic moieties are more reactive than the two terminal parts. Most interestingly, oligomers BN2, BN3, and BN4 display nodal-shaped HOMOs with boundaries at the BN units. This suggests that the conjugation extension in the vertical backbone is more pronounced on the effective conjugation length than the other horizontal one. The calculated energies, oscillator strength, and compositions of major electronic transitions are shown in the Supporting Information, Tables S5–S8 and the calculated HOMO–LUMO levels for the oligomers are consistent with those experimentally determined values.

Oxidations of the BN-Embedded PAHs

Apart from the coordination with fluoride ions, the as-prepared BN-embedded PAH oligomers can be oxidized since the sulfur in thiophene rings can be easily oxidized into sulfoxide and further to sulfone. As shown in Scheme 3, the

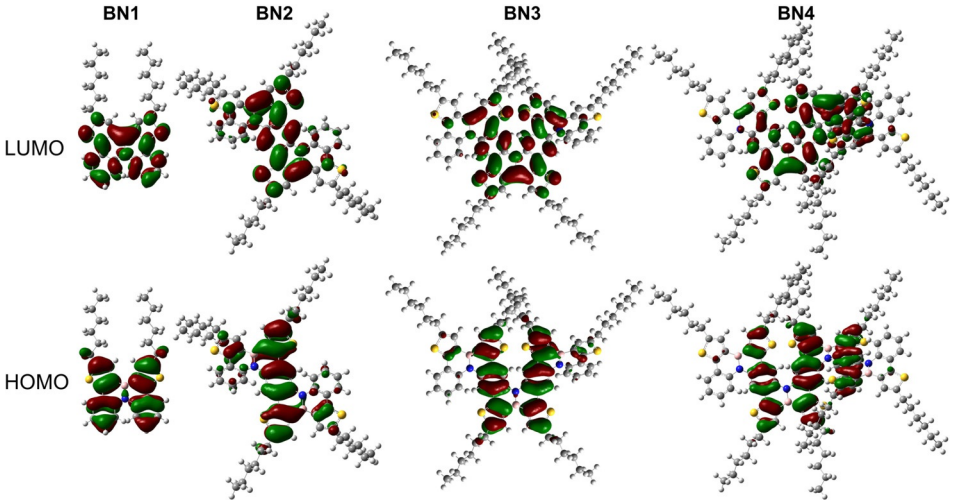

Figure 8. Calculated frontier orbitals of BN-embedded PAH oligomers BN1–BN4.

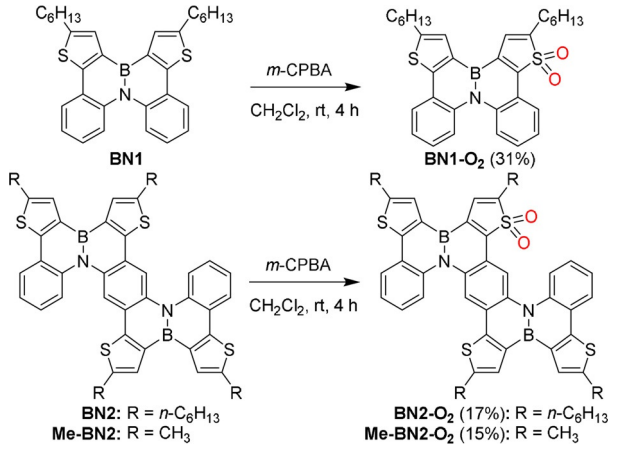

Scheme 3. Oxidation of the BN-embedded PAHs.

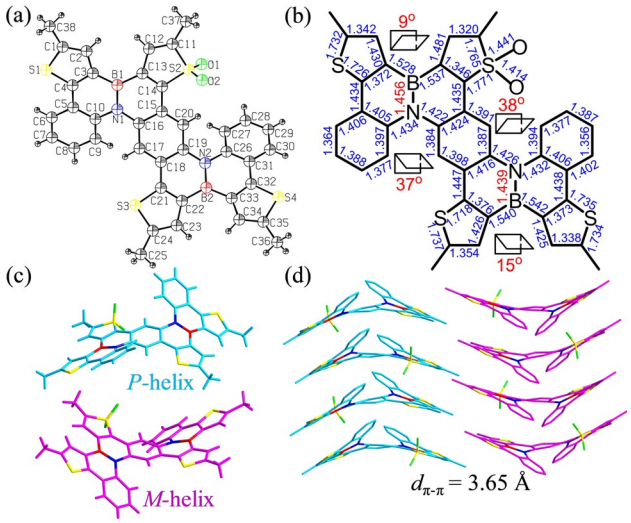

Figure 9. a) ORTEP drawing of Me-BN2-O_2 with ellipsoids set at 50% probability. b) Selected bond lengths for Me-BN2-O_2. c) *P*- and *M*-helical structures of Me-BN2-O_2. d) Crystal packing of Me-BN2-O_2 (Hydrogen atoms are omitted for clarity).[30]

oxidation reaction was performed by stirring the mixture of BN1 and *meta*-chloroperoxybenzoic acid (*m*-CPBA) in DCM at room temperature. A sulfone compound BN1-O_2 was obtained as the major product. The successful oxidation of only one thiophene ring was verified by its asymmetric aromatic structure in the low-field region of the ^{1}H NMR spectrum (Supporting Information, Figure S44). The oxidation of sulfur into sulfone instead of sulfoxide was proved by HRMS spectroscopy. Moreover, the delocalization of the HOMOs and LUMOs in the inner parts of the BN-embedded PAH oligomers suggest that the inner parts are more active than the outer parts although less steric hindrance may be found for the two terminal sides of the oligomers. To verify this assumption, BN2 was also chosen to carry out the oxidation reaction since two environmentally different thiophene rings can be found in the skeleton of BN2, that is, two thiophene rings in the outer part and two in the inner part. As shown in Scheme 3, under the same condition, a sulfone compound BN2-O_2 was obtained as the major product. The relatively low isolated yield for the oxidized product is due to the extremely close polarities of the other mono-oxidized by-products. Moreover, the mono-oxidized products can be further oxidized into multiple oxidized species by simply feeding more *m*-CPBA. However, no selectivity can be found for the second oxidation due to the dramatically changed frontier orbitals of the mono-oxidized products.

To further confirm the oxidation at the inner thiophene rings and exclude the formation of two sulfoxide units, single-crystal X-ray diffraction analysis was performed. Similar to Me-BN2, methyl substituted analogue Me-BN2-O_2 was synthesized under the same condition and the single crystal was obtained by slow solvent diffusion method. As shown in Figure 9, the backbone of Me-BN2-O_2 adopts a twisted conformation similar to Me-BN2. However, upon oxidation, the molecules alignments changes from a monoclinic system for Me-BN2 to an orthorhombic system for Me-BN2-O_2. Moreover, the length of the B–N bond in the azaborine ring fused on the thiophene dioxide ring slightly changes from 1.454(3) to 1.456(3) Å, confirming their essentially double-bond character. In comparison to the negligible change of the B–N bond, however, the length of the C–C bond shared by the thiophene dioxide and the neighboring azaborine rings decreases from 1.379(3) to 1.346(6) Å. Thus, the shortened bond may significantly affect the aromaticity of the aromatic rings. As shown in Figure 10, the calculated NICS(1) value of the oxidized thiophene ring changes from −9.4 to −0.9 ppm, which is obviously due to the loss of two π electrons on sulfur atom. Moreover, the neighboring azaborine ring becomes more aromatic with the NICS(1) value reducing from −3.7 to −4.6 ppm. This suggests that the oxidation has a strong influence on the aromaticity of the surrounded aromatic rings. Furthermore, although the oxidized product Me-BN2-O_2 exhibits an asymmetric structure, two types of cove regions with similar distortion angels can be observed in comparison to Me-BN2 (Figure 9b). Furthermore, both *P*- and *M*-helical structures can be found in the single crystal of Me-BN2-O_2 (Figure 9c). However, unlike Me-BN2, the *P*- or *M*-helical structures are arranged in an offset face-to-face stacking array

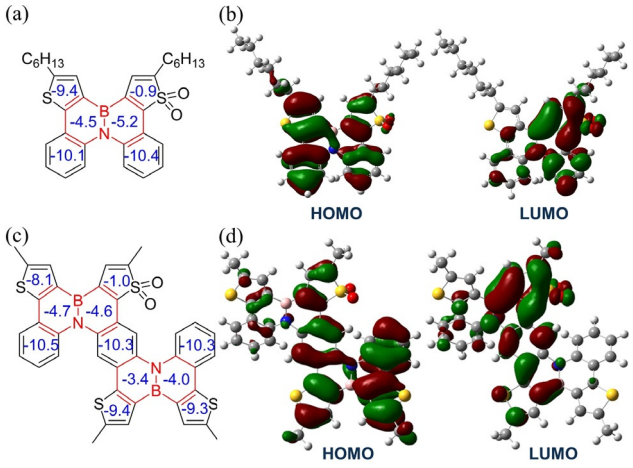

Figure 10. Calculated NICS(1) values (in ppm, a and c) and frontier orbitals (b and d) of BN1-O_2 and Me-BN2-O_2.

with a π–π distance of 3.65 Å (Figure 9d). All these single crystal structure date further confirm our assumption that the inner parts of the BN-embedded PAH oligomers are more active than the outer parts.

Furthermore, the oxidation product BN2-O_2 displays absorption and PL maxima at 455 and 522 nm in THF solution (Supporting Information, Figures S8 and S9). Unlike BN1 and BN2, the solvatochromic effects of which are very weak, significant solvent-dependent PL spectra can be found for both BN1-O_2 and BN2-O_2. A bathochromic shift of 78 and 56 nm of the maximum PL wavelength can be observed for BN1-O_2 and BN2-O_2, respectively, when the solvent polarity increased from hexane (462 nm for BN1-O_2 and 492 nm for BN2-O_2) to *N*,*N*-dimethylformamide (540 nm for BN1-O_2 and 548 nm for BN2-O_2). Such a bathochromic shift is characteristic of an efficient charge transfer from the electron-donating moiety to the electron-withdrawing moiety. As shown in Figure 10, significant separation of the HOMO and LUMO can be found for both BN1-O_2 and BN2-O_2, which indicates the notable ICT interactions in the oxidized products. Therefore, these results suggest that the oxidation has a significant effect on the ICT interactions in these BN-embedded PAH oligomers.

Conclusion

We report the straightforward synthesis of four BN-embedded oligomers via electrophilic borylation processes. In this method, multiple pairs of BN units up to four have been successfully incorporated in the large polycyclic aromatic hydrocarbons. Single-crystal X-ray analysis indicates the delocalized BN double bond characteristics in these PAH oligomers. The photophysical, electrochemical, and theoretical approaches further reveal that the conjugation can be extended through the azaborine rings. Moreover, the delocalization of frontier orbitals and the relatively lower aromaticity in the inner moieties of the BN-embedded PAH oligomers suggest that the inner parts are more active than the outer parts, which is further verified by a simple oxidation reaction. Most interestingly, the oxidation has significant effects on the aromaticity and the ICT interactions in these BN-embedded PAHs. Overall, this work may help to understand the intriguing electronic and optical properties of the BN-containing aromatics and provide a pathway for designing BN-embedded PAHs for further optoelectronic applications.

Acknowledgements

This work was financially supported by the National Natural Science Foundation of China (21674023, 51722301, 51903052, and 21733003), Shanghai Pujiang Project (19PJ1400700), and National Key R&D Program of China (2018YFA0209401).

Conflict of interest

The authors declare no conflict of interest.

Keywords: aromaticity · azaborine · heterocycles · oligomers · polycyclic aromatic hydrocarbons

How to cite: *Angew. Chem. Int. Ed.* **2020**, *59*, 7122–7130
Angew. Chem. **2020**, *132*, 7188–7196

[1] a) C. W. Tang, S. A. VanSlyke, *Appl. Phys. Lett.* **1987**, *51*, 913–915; b) M. C. Gather, A. Köhnen, K. Meerholz, *Adv. Mater.* **2011**, *23*, 233–238; c) A. C. Grimsdale, K. L. Chan, R. E. Martin, P. G. Jokisz, A. B. Holmes, *Chem. Rev.* **2009**, *109*, 897–1091; d) J. Huang, J.-H. Su, H. Tian, *J. Mater. Chem.* **2012**, *22*, 10977–10989; e) T. Hatakeyama, K. Shiren, K. Nakajima, S. Nomura, S. Nakatsuka, K. Kinoshita, J. Ni, Y. Ono, T. Ikuta, *Adv. Mater.* **2016**, *28*, 2777–2781.

[2] a) M. Bendikov, F. Wudl, D. F. Perepichka, *Chem. Rev.* **2004**, *104*, 4891–4946; b) J. Wu, W. Pisula, K. Müllen, *Chem. Rev.* **2007**, *107*, 718–747; c) Y. Wang, Z. Yan, H. Guo, M. A. Uddin, S. Ling, X. Zhou, H. Su, J. Dai, H. Y. Woo, X. Guo, *Angew. Chem. Int. Ed.* **2017**, *56*, 15304–15308; *Angew. Chem.* **2017**, *129*, 15506–15510; d) M. Chu, J.-X. Fan, S. Yang, D. Liu, C. F. Ng, H. Dong, A.-M. Ren, Q. Miao, *Adv. Mater.* **2018**, *30*, 1803467; e) Z. Jin, Z.-F. Yao, K. P. Barker, J. Pei, Y. Xia, *Angew. Chem. Int. Ed.* **2019**, *58*, 2034–2039; *Angew. Chem.* **2019**, *131*, 2056–2061.

[3] a) C. Li, M. Liu, N. G. Pschirer, M. Baumgarten, K. Müllen, *Chem. Rev.* **2010**, *110*, 6817–6855; b) G. Li, R. Zhu, Y. Yang, *Nat. Photonics* **2012**, *6*, 153–161; c) H. Fu, Z. Wang, Y. Sun, *Angew. Chem. Int. Ed.* **2019**, *58*, 4442–4453; *Angew. Chem.* **2019**, *131*, 4488–4499; d) Z. Yao, X. Liao, K. Gao, F. Lin, X. Xu, X. Shi, L. Zuo, F. Liu, Y. Chen, A. K.-Y. Jen, *J. Am. Chem. Soc.* **2018**, *140*, 2054–2057.

[4] a) M. Stępień, E. Gońka, M. Żyła, N. Sprutta, *Chem. Rev.* **2017**, *117*, 3479–3716; b) Q. Miao, *Adv. Mater.* **2014**, *26*, 5541–5549; c) X.-Y. Wang, X. Yao, A. Narita, K. Müllen, *Acc. Chem. Res.* **2019**, *52*, 2491–2505.

[5] a) K. Matsuo, S. Saito, S. Yamaguchi, *J. Am. Chem. Soc.* **2014**, *136*, 12580–12583; b) J. M. Farrell, C. Mützel, D. Bialas, M. Rudolf, K. Menekse, A.-M. Krause, M. Stolte, F. Würthner, *J. Am. Chem. Soc.* **2019**, *141*, 9096–9104; c) H. Yokoi, Y. Hiraoka, S. Hiroto, D. Sakamaki, S. Seki, H. Shinokubo, *Nat. Commun.* **2015**, *6*, 8215.

[6] a) Z. Liu, T. B. Marder, *Angew. Chem. Int. Ed.* **2008**, *47*, 242–244; *Angew. Chem.* **2008**, *120*, 248–250; b) M. J. D. Bosdet, W. E. Piers, *Can. J. Chem.* **2009**, *87*, 8–29.

[7] a) T. Hatakeyama, S. Hashimoto, S. Seki, M. Nakamura, *J. Am. Chem. Soc.* **2011**, *133*, 18614–18617; b) X.-Y. Wang, A. Narita, X. Feng, K. Müllen, *J. Am. Chem. Soc.* **2015**, *137*, 7668–7671; c) X.-Y. Wang, F.-D. Zhuang, R.-B. Wang, X.-C. Wang, X.-Y. Cao, J.-Y. Wang, J. Pei, *J. Am. Chem. Soc.* **2014**, *136*, 3764–3767.

[8] a) C. R. McConnell, S.-Y. Liu, *Chem. Soc. Rev.* **2019**, *48*, 3436–3453; b) F.-D. Zhuang, Z.-H. Sun, Z.-F. Yao, Q.-R. Chen, Z. Huang, J.-H. Yang, J.-Y. Wang, J. Pei, *Angew. Chem. Int. Ed.* **2019**, *58*, 10708–10712; *Angew. Chem.* **2019**, *131*, 10818–10822; c) H. Huang, Y. Zhou, M. Wang, J. Zhang, X. Cao, S. Wang, D. Cao, C. Cui, *Angew. Chem. Int. Ed.* **2019**, *58*, 10132–10137; *Angew. Chem.* **2019**, *131*, 10238–10243; d) S. Nakatsuka, N. Yasuda, T. Hatakeyama, *J. Am. Chem. Soc.* **2018**, *140*, 13562–13565; e) X. Long, D. Li, B. Wang, Z. Jiang, W. Xu, B. Wang, D. Yang, Y. Xia, *Angew. Chem. Int. Ed.* **2019**, *58*, 11369–11373; *Angew. Chem.* **2019**, *131*, 11491–11495; f) Y. Min, C. Dou, H. Tian, Y. Geng, J. Liu, L. Wang, *Angew. Chem. Int. Ed.* **2018**, *57*,

2000 – 2004; *Angew. Chem.* **2018**, *130*, 2018 – 2022; g) Y. Min, C. Dou, D. Liu, H. Dong, J. Liu, *J. Am. Chem. Soc.* **2019**, *141*, 17015 – 17021.
[9] a) Z. X. Giustra, S.-Y. Liu, *J. Am. Chem. Soc.* **2018**, *140*, 1184 – 1194; b) X.-Y. Wang, J.-Y. Wang, J. Pei, *Chem. Eur. J.* **2015**, *21*, 3528 – 3539; c) K. Matsui, S. Oda, K. Yoshiura, K. Nakajima, N. Yasuda, T. Hatakeyama, *J. Am. Chem. Soc.* **2018**, *140*, 1195 – 1198; d) X. Wang, F. Zhang, K. S. Schellhammer, P. Machata, F. Ortmann, G. Cuniberti, Y. Fu, J. Hunger, R. Tang, A. A. Popov, B. Berger, K. Müllen, X. Feng, *J. Am. Chem. Soc.* **2016**, *138*, 11606 – 11615; e) S. Tsuchiya, H. Saito, K. Nogi, H. Yorimitsu, *Org. Lett.* **2019**, *21*, 3855 – 3860.
[10] Y. L. Rao, H. Amarne, L. D. Chen, M. L. Brown, N. J. Mosey, S. Wang, *J. Am. Chem. Soc.* **2013**, *135*, 3407 – 3410.
[11] a) C. Zhu, A. J. Kalin, L. Fang, *Acc. Chem. Res.* **2019**, *52*, 1089 – 1100; b) G. Zhou, M. Baumgarten, K. Müllen, *J. Am. Chem. Soc.* **2007**, *129*, 12211 – 12221; c) P. M. Burrezo, X. Zhu, S.-F. Zhu, Q. Yan, J. T. L. Navarrete, H. Tsuji, E. Nakamura, J. Casado, *J. Am. Chem. Soc.* **2015**, *137*, 3834 – 3843.
[12] A. W. Baggett, F. Guo, B. Li, S.-Y. Liu, F. Jäkle, *Angew. Chem. Int. Ed.* **2015**, *54*, 11191 – 11195; *Angew. Chem.* **2015**, *127*, 11343 – 11347.
[13] a) G. Zhou, M. Baumgarten, K. Müllen, *J. Am. Chem. Soc.* **2008**, *130*, 12477 – 12484; b) X. Lu, S. Fan, J. Wu, X. Jia, Z.-S. Wang, G. Zhou, *J. Org. Chem.* **2014**, *79*, 6480 – 6489.
[14] a) A. M. Genaev, S. M. Nagy, G. E. Salnikov, V. G. Shubin, *Chem. Commun.* **2000**, 1587 – 1588; b) Y. Chen, W. Chen, Y. Qiao, G. Zhou, *Chem. Eur. J.* **2019**, *25*, 9326 – 9338; c) T. S. De Vries, A. Prokofjevs, J. N. Harvey, E. Vedejs, *J. Am. Chem. Soc.* **2009**, *131*, 14679 – 14687.
[15] A. S. Guram, S. L. Buchwald, *J. Am. Chem. Soc.* **1994**, *116*, 7901 – 7902.
[16] N. Miyaura, A. Suzuki, *Chem. Rev.* **1995**, *95*, 2457 – 2483.
[17] X. Wang, F. Zhang, J. Liu, R. Tang, Y. Fu, D. Wu, Q. Xu, X. Zhuang, G. He, X. Feng, *Org. Lett.* **2013**, *15*, 5714 – 5717.
[18] A. J. Ashe III, *Organometallics* **2009**, *28*, 4236 – 4248.
[19] E. R. Abbey, L. N. Zakharov, S.-Y. Liu, *J. Am. Chem. Soc.* **2008**, *130*, 7250 – 7252.
[20] Z. Chen, C. S. Wannere, C. Corminboeuf, R. Puchta, P. v. R. Schleyer, *Chem. Rev.* **2005**, *105*, 3842 – 3888.
[21] J. Lee, H. Li, A. J. Kalin, T. Yuan, C. Wang, T. Olson, H. Li, L. Fang, *Angew. Chem. Int. Ed.* **2017**, *56*, 13727 – 13731; *Angew. Chem.* **2017**, *129*, 13915 – 13919.
[22] M. Kastler, J. Schmidt, W. Pisula, D. Sebastiani, K. Müllen, *J. Am. Chem. Soc.* **2006**, *128*, 9526 – 9534.
[23] a) F. Jäkle, *Chem. Rev.* **2010**, *110*, 3985 – 4022; b) T. W. Hudnall, C.-W. Chiu, F. P. Gabbaï, *Acc. Chem. Res.* **2009**, *42*, 388 – 397.
[24] J. Pommerehne, H. Vestweber, W. Guss, R. F. Mahrt, H. B-ssler, M. Porsch, J. Daub, *Adv. Mater.* **1995**, *7*, 551 – 554.
[25] H. Fallah-Bagher-Shaidaei, C. S. Wannere, C. Corminboeuf, R. Puchta, P. v. R. Schleyer, *Org. Lett.* **2006**, *8*, 863 – 866.
[26] H. Kalam, A. Kerim, K. Najmidin, P. Abdurishit, T. Tawar, *Chem. Phys. Lett.* **2014**, *592*, 320 – 325.
[27] M. J. Frisch, G. W. Trucks, H. B. Schlegel, G. E. Scuseria, M. A. Robb, J. R. Cheeseman, J. A. Montgomery, T. Vreven, K. N. Kudin, J. C.Burant, J. M. Millam, S. S. Iyengar, J. Tomasi, V. Barone, B. Mennucci, M. Cossi, G. Scalmani, N. Rega, G. A. Petersson, H. Nakatsuji, M. Hada, M. Ehara, K. Toyota, R. Fukuda, J. Hasegawa, M. Ishida, T. Nakajima, Y. Honda, O. Kitao, H. Nakai, M. Klene, X. Li, J. E. Knox, H. P. Hratchian, J. B. Cross, V. Bakken, C. Adamo, J. Jaramillo, R. Gomperts, R. E. Stratmann, O. Yazyev, A. J. Austin,R. Cammi, C. Pomelli, J. W. Ochterski, P. Y. Ayala, K. Morokuma, G. A. Voth, P. Salvador, J. J. Dannenberg, V. G. Zakrzewski, S. Dapprich, A. D. Daniels, M. C. Strain, O. Farkas, D. K. Malick, A. D. Rabuck, K. Raghavachari, J. B. Foresman, J. V. Ortiz, Q. Cui, A. G. Baboul, S. Clifford, J. Cioslowski, B. B. Stefanov, G. Liu, A. Liashenko, P. Piskorz, I. Komaromi, R. L. Martin, D. J. Fox,T. Keith, Al M. A. Laham, C. Y. Peng, A. Nanayakkara, M. Challacombe, P. M. W. Gill, B. Johnson, W. Chen, M. W. Wong,C. Gonzalez, J. A. Pople. Gaussian 03, revision C.02.Gaussian, Inc., Wallingford, CT **2004**.
[28] a) P. Chen, A. S. Marshall, S.-H. Chi, X. Yin, J. W. Perry, F. Jäkle, *Chem. Eur. J.* **2015**, *21*, 18237 – 18247; b) L. Ji, S. Griesbeck, T. B. Marder, *Chem. Sci.* **2017**, *8*, 846 – 863.
[29] G. Li, Y. Chen, Y. Qiao, Y. Lu, G. Zhou, *J. Org. Chem.* **2018**, *83*, 5577 – 5587.
[30] CCDC 1586441, 1954993, and 1954995 (BN1, Me-BN2, and Me-BN2-O_2) contain the supplementary crystallographic data for this paper. These data are provided free of charge by The Cambridge Crystallographic Data Centre.

Manuscript received: January 12, 2020
Accepted manuscript online: February 17, 2020
Version of record online: March 10, 2020

